Fuel 340 (2023) 127467

Contents lists available at ScienceDirect

Fuel

journal homepage: www.elsevier.com/locate/fuel

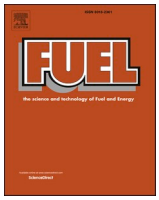

Full Length Article

The influence of different fuels and injection methods of RCCI and DCI in hybrid ICE-Battery vehicle performance

Hadi Taghavifar

Department of Technology and Safety, UiT the Arctic University of Norway, Tromsø, Norway

ARTICLE INFO

Keywords:
Battery
HEV
Hydrogen
RCCI
Thermal performance

ABSTRACT

The incorporation of two recent technologies of using the dual-fuel reactivity controlled compression ignition (RCCI) combustion engine within the hybrid electric vehicle (HEV) is practiced to show how this combination can reduce the emission and enhance the thermal efficiency of the system. In particular, the heat transfers from the engine wall and the exhaust heat flow from the engine under different injection modes and fuels are of interest. The study in terms of thermal performance, fuel consumption, and battery state of charge (SOC) focuses mainly on the comparison between three cases of D100 (pure diesel) as the reference (baseline conventional direct pure diesel injection) case, D80H20 (80% diesel, 20% hydrogen) direct co-injection (DCI), and D80H20 RCCI (port + direct dual fuel injection). The NOx emission and engine power in the simulated drive cycle are investigated where the battery capacity and D50M50 (direct co-injection of 50% diesel with 50% methanol) are the additional cases. The findings indicate that the Battery SOC is preserved in better condition when the RCCI mode engine is coupled in the hybrid vehicle. The piston wall heat flux for D80H20 in DCI increases by 45.2% and for the RCCI increases by 60.5% compared to baseline diesel injection mode. It is also proved that the HEV releases considerably lower NOx compared to DCI and more NOx compared to D100 and D50M50.

1. Introduction

The automotive industry along with the energy crisis advent has shifted towards the use of non-fossil fuels and electrical power use. There are also the environmental concerns that mandates inauguration of new regulations to control the amount of emissions from the tailpipe and the exhaust systems. The immediate transition to all electric vehicle in a short prospect does not seem to be a viable plan in all energy sectors and in particular in the transportation (mainly due to the shortcomings in terms of the infrastructure and lack of clean electric energy resources) [1,2]. Therefore, the use of electric plus engine hybrid mode is inevitable in the short term. However, the engine that is to be used in the hybrid powertrain configuration needs to be aligned with the utmost progressed combustion mode in dual-fuel operation with the promising alternative fuels. Meanwhile, the ability to control the combustion intensity and the flexibility to handle the thermal performance in the combustion engine by two different fuels characterized by different reaction ability is introduced in the reactivity controlled compression ignition (RCCI) engine via low temperature combustion (LTC) [3–5].

Hydrogen is one of the potential green fuels to be used in the engine since it offers very-low emission species when blended with other conventional fuels such as diesel and by having the high calorific value, high flame propagation speed and low ignition energy hydrogen can boost the thermal efficiency [6,7]. Nevertheless, the use of pure hydrogen-powered vessel is not recommended and has not been yet reached to the commercial stage due to challenges of backfire, liquidation, storing, and refilling. Therefore, hydrogen is mostly investigated in a dual-fuel engine with a hydrocarbon fuel to cope with the hydrogen engine issues [8]. Methanol is also a viable fuel to be used in the RCCI method because of high octane number, high flame speed, and heat of vaporization [9,10].

In order to comply with the stringent emission regulations, the electrification strategy of the navigation fleet [11] should be adopted in addition to the RCCI engine. In this regard, the engine/battery/FC are hybridized in the series or parallel array [12]. The hybrid powertrain allows for the reduced size of the engine and the power sizing of fuel cell/engine parallel hybrid in the hybrid range extender are provided in [13]. Garcia et al. [14] investigated the potential of the RCCI engine in a parallel hybrid vehicle on emission reduction framework of 2025. Their work targeted reduction of global CO2 and local soot and NOx by incorporating the advanced combustion RCCI (with diesel and gasoline) and the hybrid battery powering mode. The hybrid electric vehicles (HEV) are studied nowadays extensively and the shifting the power and energy flow via energy management and controlling methods between energy source elements have gained enormous attention [15–17]. There are interesting researches on the RCCI + Battery in the literature that are pushing towards ultimate low emissions. Garcia et al. [18] reported the RCCI series hybrid truck experiment in terms of energy performance and

https://doi.org/10.1016/j.fuel.2023.127467
Received 5 October 2022; Received in revised form 4 January 2023; Accepted 7 January 2023
Available online 16 January 2023

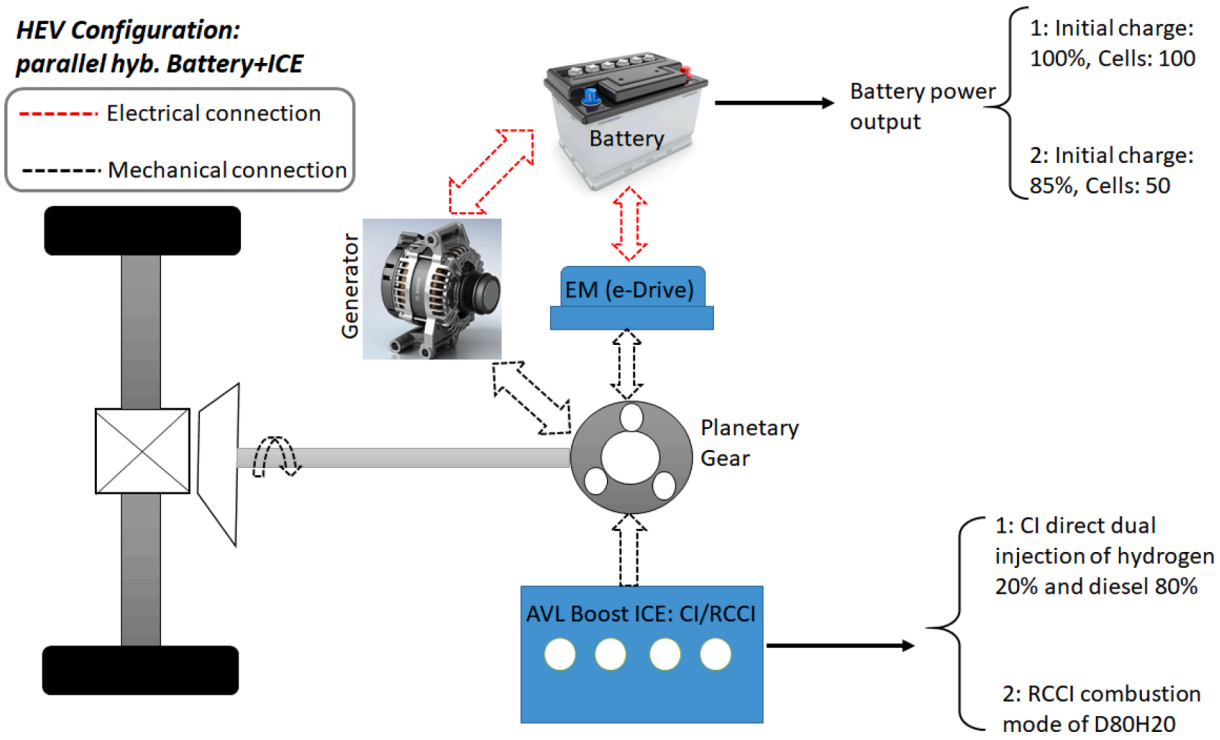

Fig. 1. Schematic representation of the proposed drivetrain configuration in two cases of interest.

CO2 reduction in a transient real drive setup. With employment of the wide calibration map and transient tests, the measurements showed the same battery requirement of powertrain configuration under different fueling condition and start of combustion (SOC) while 3.3% CO2 tail-pipe reduction of dual-fuel RCCI mode compared to baseline conventional diesel combustion (CDC) is resulted. Climent et al. [19] used the spark-ignition (SI) in the hybrid series electric powertrain to examine the effect of the exhaust gas recirculation (EGR) on fuel consumption drop. This research indicated that in the hybrid powertrain EGR effect is more pronounced in fuel economy up to 4.6% and EGR led to 2.6% fuel consumption benefit compared to the conventional non-electric vehicles. Benajes et al. [20] considered the RCCI plug-in HEV to review the extent of emission reduction where they concluded 30% reduction of CO2 in life cycle assessment format. Their results also demonstrated ultra-low NOx and soot emission achievement. The RCCI is mostly recognized beneficial to meet the Euro 6 soot standard.

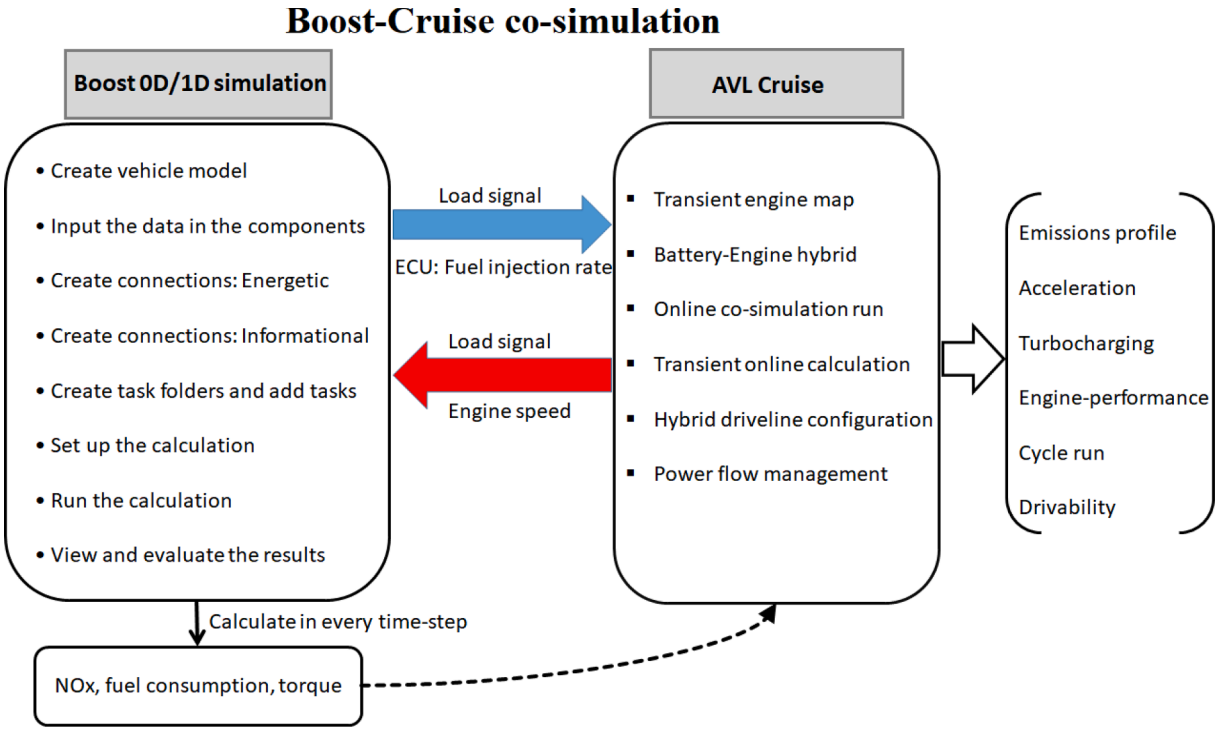

Fig. 2. Workflow of avl-boost and avl-cruise coupling via the load signal for the battery-ice hev model.

Table 1
General vehicle parameters.

Curb weight	1260.0 kg
Vehicle mass	1315.0 kg
Wheel base	2550.0 mm
Frontal area	1.75 m^2
Drag coefficient	0.3
Stat. rolling radius	287.0 mm
Dyn. Rolling radius	292.0 mm
Boost engine Max. power	122.84 kW

This attempt introduces a 0D-1D modeling of the hybrid powertrain and driveline of the engine and driveline of a parallel hybrid electric vehicle with conventional direct co-injection and port-direct injection of different fuels. The scrutiny of the bibliography of the technical publications show no record on the hybrid ICE/battery vehicle where the injection mode and battery capacity under different fuels considered on the emission and power performance of the vehicle. The propriety of dual-fuel ICE with battery hybrid either as direct co-injection or the RCCI mode with diesel/hydrogen, diesel/methanol, and single fuel powered vehicle are proposed and the thermal performance and emission reduction of such powertrain presented transiently during the new European driving cycle (NEDC). The comparison is made between the conventional diesel combustion (CDC), dual fuel direct co-injection (DCI), and dual fuel RCCI for D100 and D80H20 fuels. Under this situation, the state of the charge of battery (SOC) and the battery performance when ICE operates with the above parameters opens pathway for a more realistic hybrid electric vehicle. Moreover, the effect of the battery capacity and the initial charge in the emission and power delivery of the proposed architecture of the vehicle is represented in this research. A brief schematic illustration of three proposed cases of study is shown in Fig. 1.

2. Powertrain and driveline modeling

The IC engine modeled via AVL boost with corresponding components is modeled by thermodynamic cycle simulation, in which gas dynamic and heat transfer principles are incorporated for detailed output data as signal load. The information in each time step feeds to hybrid driveline consisting of electric and mechanical connections to drive the investigated vehicle in the AVL Cruise platform. The interaction of battery and engine (from the engine thermodynamic simulation interface) enables the vehicle performance assessment in variety of engine operation in terms of fuel injection and fuel type modification. In current research, the hydrogen, methane, and diesel are used in the AVL boost engine element while the fuel injection and combustion method of dual-fuel direct injection as well as the RCCI (port indirect plus direct injection with different fuels of reactivity) are practiced. The flowchart representation of AVL boost-AVL cruise coupling is depicted in Fig. 2.

2.1. Vehicle simulation (AVL Cruise)

The vehicle element is essential part of driveline configuration and the system assembly, which includes the car dimension and weight characteristics (mentioned in Table 1) [21].

The superposition of forces on the vehicle is computable based on the

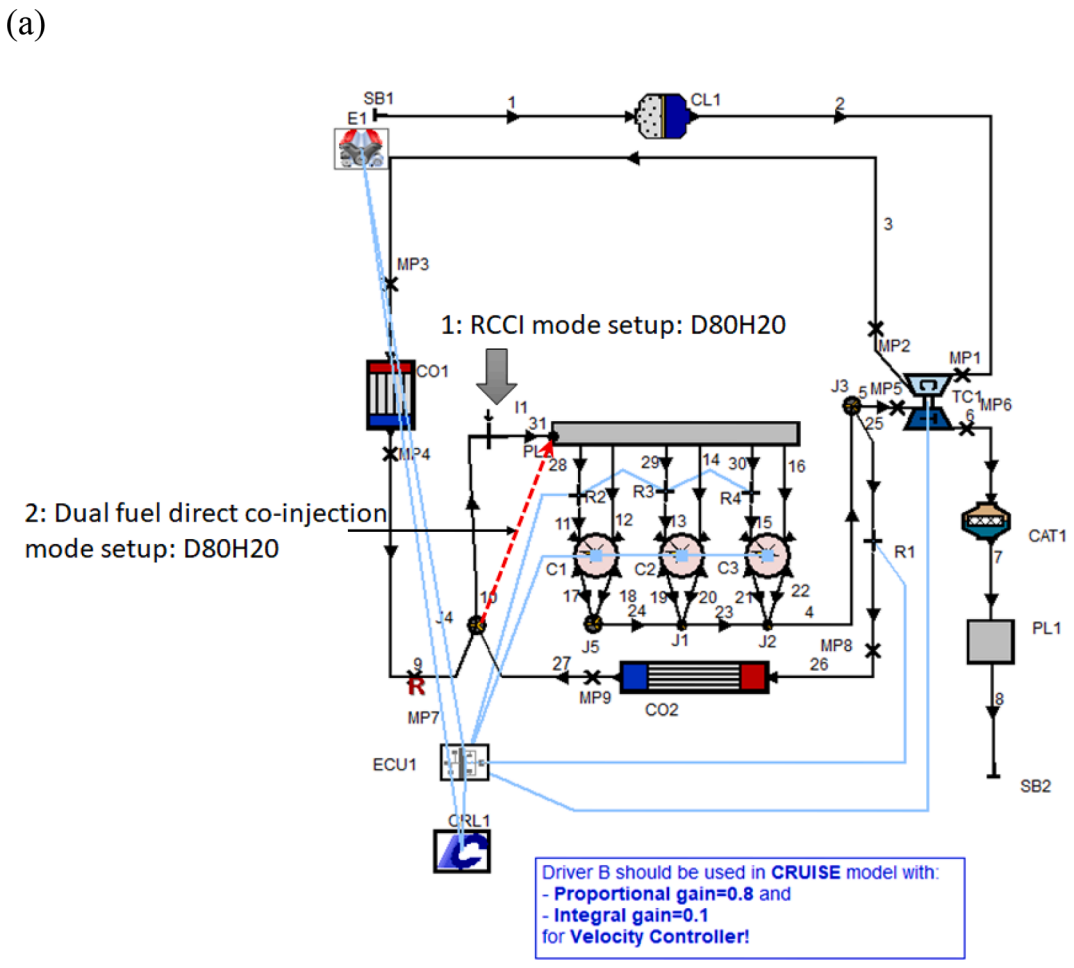

Fig. 3. (a) The injection line of fuel and the engine cycle in the AVL Boost with ECU and the cruise link (CRL), (b) the structure of the Boost engine interface/component in the AVL Cruise powertrain.

(b)

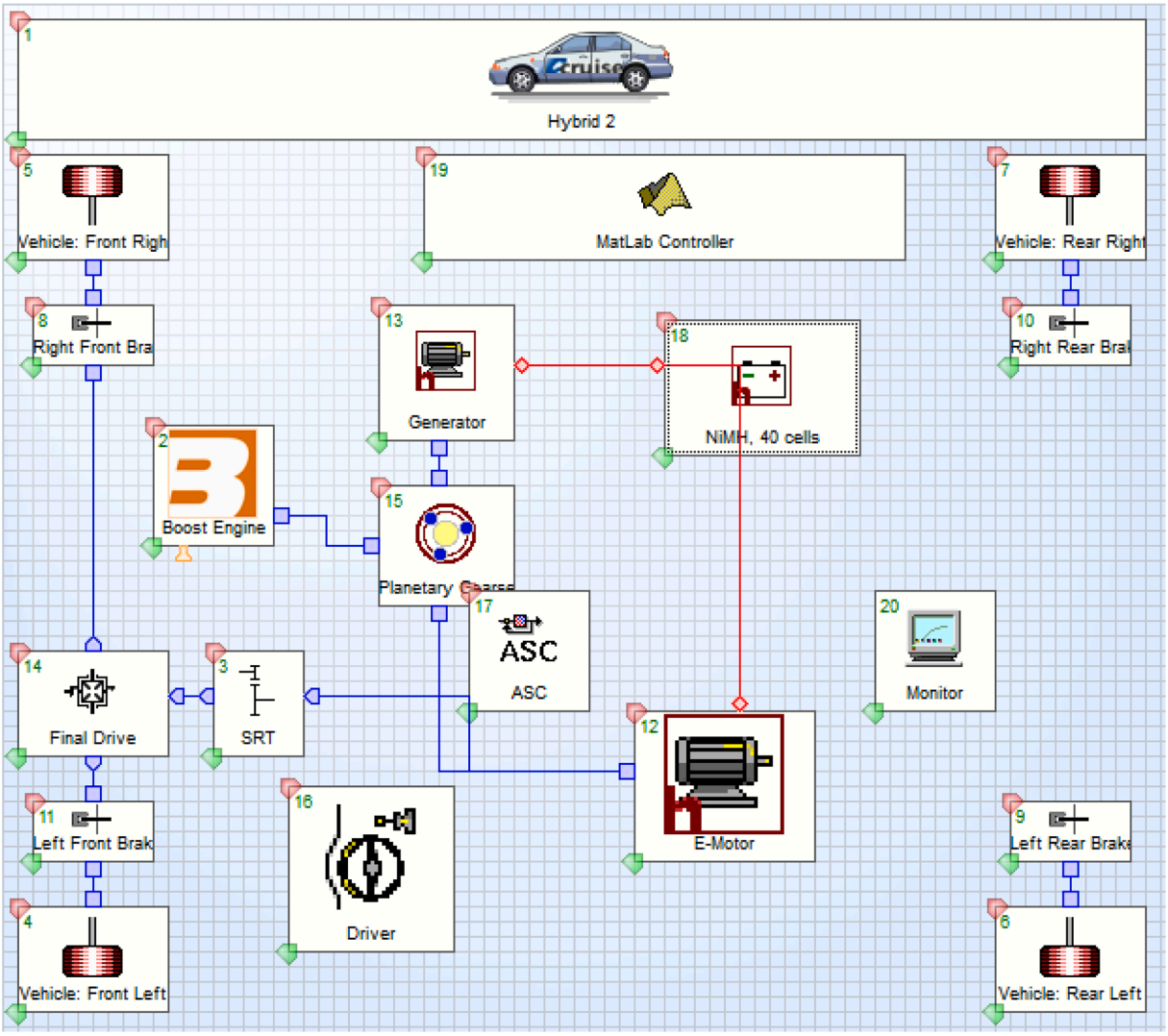

Fig. 3. (*continued*).

road resistance and wheel load (motion data: aerodynamic drag coefficient, acceleration, etc.) [22]. The balance equation considering a rear drive powertrain and variant velocity profile on a rectilinear road of α_p slope with respect to horizontal line gives [23]:

$$F_t - G_a \sin\alpha_p - R_t - R_a - R_{rul1} - R_{rul2} - R_{i1} - R_{i2} = 0 \quad (1)$$

The resistant forces induced by the wheels' inertia are characterized by R_{i1} and R_{i2}. Further, F_t represents the traction force (N), and R_{rul} is the total rolling resistance, the slope climb resistance is given by ($R_p = G_a$. Sin α_p), and Ra is the acceleration resistance.

The assembled engine unit comprised of a turbocharger, air cleaner, plenum, catalyst, ECU (engine control unit), cylinders, and air cooler is depicted in Fig. 3a. This engine unit is shown in Boost engine interface element of AVL cruise software. The fuel injection in Fig. 3a is managed in two configurations; case 1 shows the port injection of the first type of fuel and direct injection of the second type of fuel. While in case 2, there is a dual-fuel direct injection of two different types of fuels. The output data from the Boost engine is transferred to a vehicle simulation in the AVL cruise by load signal in each time step in transient mode. The AVL cruise structure in co-powering engine-battery driveline that calls Boost interface for engine calculation is shown in Fig. 3b. For the control of the power split and the energy management between main components, the built-in MATLAB/SIMULINK controller strategy is utilized that is emplaced within the AVL/CRUISE model as an executable .DLL code.

Table 2
Input data of the vehicle elements' operational parameters.

Generator/E-Motor	
Nominal voltage	288.0 V
Max. speed	8000.0 1/min
Max. current-Generator	300.0 A
Mass of machine	32.7 kg
Max. temperature	95.0 °C
Planetary gear	
Base ratio	2.6
Inertia moment sun/ring gear	0.0015 kg.m^2
Single ratio transmission (SRT)	
Transmission ratio	3.905
Final Drive	
Torque split factor	1.0

The Boost engine is intended for the transient calculation of load signal, fuel consumption, and NOx maps. The inertia moment is set to 0.2 kg.m^2, with the engine speed limits of idle speed equal to 800.0 1/min and maximum speed equal to 4000.0 1/min. The planetary gear is used to adjust the generated power from the engine and battery then

Table 3
Battery NiMH 40 cells operating condition.

Max. charge	6.5 Ah
Nominal voltage	7.2 V
Initial charge	58.0%
Number of cells per cell-row	40
Mass of a cell	0.9979 kg
Operating temperature	25.0 ℃
Internal charge resistance	0.0197 Ohm
Internal discharge resistance	0.0269 Ohm

deliver it to Final Drive element and then to the rear axle. The designed driveline allows recharging of the battery through generator and E-Motor elements, in which the mechanical energy flow is turned into the electric energy and stored in the battery. The battery and engine provide power in hybrid parallel arrangement. The "MATLAB Controller" element allows the management of energy during the cycle run over time with different road map and imposed loads.

The tuning parameters of different elements are summarized in Table 2, while the Boost engine and battery components are further detailed in the following due to their significance in the current work.

2.2. System equations

In this section, the mathematical modeling behind each component of the system would be described.

2.2.1. Battery

Within the automotive electrical system, the battery assumes the role of a chemical storage unit for the electrical energy produced by the alternator. The battery must be capable of limited-duration high-current delivery for starting (especially critical at low temperatures), and it must be able to furnish some or all of the electrical energy for other important system components for limited periods with the engine at idle or off.

The specifications of the battery as the second power source are detailed in Table 3.

At first the idle voltage $U_{Q,idle}$ and the inner resistance $R_{Q,act}$ is evaluated out of the maps for the current battery charge ($Q_{Q,act}$). The instantaneous battery current:

$$I_Q = \frac{U_{Q,net} - U_{Q,idle}}{R_{Q,act}} \tag{1}$$

The instantaneous charge of the battery is determined by means of a balance computation.

The result can be added to the existing battery charge.

$$Q_{Q,act} = Q_{Q,act-1} + \Delta t_{step}.I_Q \tag{2}$$

The internal resistance is also taken into account.

The primary structure of battery comprises a resistance and a voltage source. The dependence of resistance to temperature can be taken into account by a thermal model where the cooling and warming effects are involved in the calculations [24]. The SOC (state of charge) is one of the underlying parameters of a battery, which is described as the ratio of battery current capacity to total capacity. For the time interval dt, the varied SOC by a charging/discharging current i can be estimated by the following [25]:

$$dSOC = \frac{dQ}{Q(t)} = \frac{idt}{Q(i)} \tag{3}$$

where Q(i) represents the battery capacity of the discharging current i. Therefore, by integrating, the charging ratio is given by [25]:

$$SOC = SOC_0 - \int \frac{idt}{Q(t)} \tag{4}$$

where SOC_0 denotes the initial charge rate.

Table 4
AVL Boost setup parameters and values.

Cylinders	
Compression ratio	18
Con-Rod length	160 mm
Combustion model	AVL MCC
Number of injector holes	6
Discharge coefficient	0.82
In-cylinder swirl ratio	1.87
Air cooler	
Air cooler volume	0.8 l
Coolant temperature	300 K
ECU	
Frequency control	cyclic
Positive/negative load change	1 (1/s)

2.2.2. Combustion engine

In the transient Boost engine element, the required operational maps are produced based on the setup engine cycle simulation of AVL boost rather than stationary maps of the engine map. Therefore, an updated and online interaction of Boost Engine-Cruise results in more accurate hybrid electric powertrain output data. The details of combustion process that is the mixing controlled combustion (MCC) in the cylinder as well as fuel and gas modeling are available in [26] where the heat release and mixing rate are discussed. By using the characteristic curves/maps and external engine parameters, the engine model is described to determine the power and torque of engine, i.e. P_e and M_e [25]:

$$P_e = M_m\left[\alpha_1.\left(\frac{n_e}{n_m}\right) + \alpha_2.\left(\frac{n_e}{n_m}\right)^2 + \alpha_3.\left(\frac{n_e}{n_m}\right)^3\right](kW) \tag{5}$$

$$M_e = M_m\left[\alpha_1 + \alpha_2.\left(\frac{n_e}{n_m}\right) + \alpha_3.\left(\frac{n_e}{n_m}\right)^2\right](Nm) \tag{6}$$

where M_m corresponds to maximum power, the angular velocity of the engine is $\omega_m=(2\pi n_m)/60$ (rad/s), also $\alpha_1 + \alpha_2 + \alpha_3 = 1$ is applicable for above equations and can be estimated as [25]:

$$\alpha_1 = \frac{3-4c}{2(1-c)} = 0.75\alpha_2 = \frac{2c}{2(1-c)} = 1.5\alpha_3 = \frac{1}{2(1-c)} = -1.25 \tag{7}$$

where $c = n_M/n_m = 0.6$ is known as the elasticity coefficient and is used to calculate the maximum torque speed as $n_M = c.n_m(1/s)$, thereby the maximum torque is estimated:

$$M_M = M_m\left[\alpha_1 + \alpha_2.\left(\frac{n_M}{n_m}\right) + \alpha_3.\left(\frac{n_M}{n_m}\right)^2\right](Nm) \tag{8}$$

3. Thermodynamic engine cycle simulation (AVL Boost)

The flow from intake to the exhaust pipe through ducts by 1D finite volume is performed for the gas dynamic and heat transfer effects, meanwhile the 0D fuel injection, evaporation, and combustion phenomenon takes place within the cylinder elements [27]. The advanced RCCI and DDFI (direct dual-fuel injection) modes are simulated within AVL-Boost interface. It is important to engage in HEV efficiency when the engine runs in two different modern approach with D80H20 fuel combination. The power cycle unit consists of plenum (PL), catalyst (CAT), air cooler (CO), engine control unit (ECU), cruise link (CRL), turbocharger (TC), cylinders (C), air cleaner (CL), and measuring points (MP). The ECU component is essential since cruise controls the Boost engine via the load signal that regulates the fuel injection rate. In the cycle simulation, the species transport is handled with classic method, the special pipe discretization is performed (1D) with the average cell size of 50 mm and the end of simulation is reached at 50,000 cycles. The multi-component fuel is established within classic species setup by Boost gas properties tool, where the thermodynamic properties of each fuel

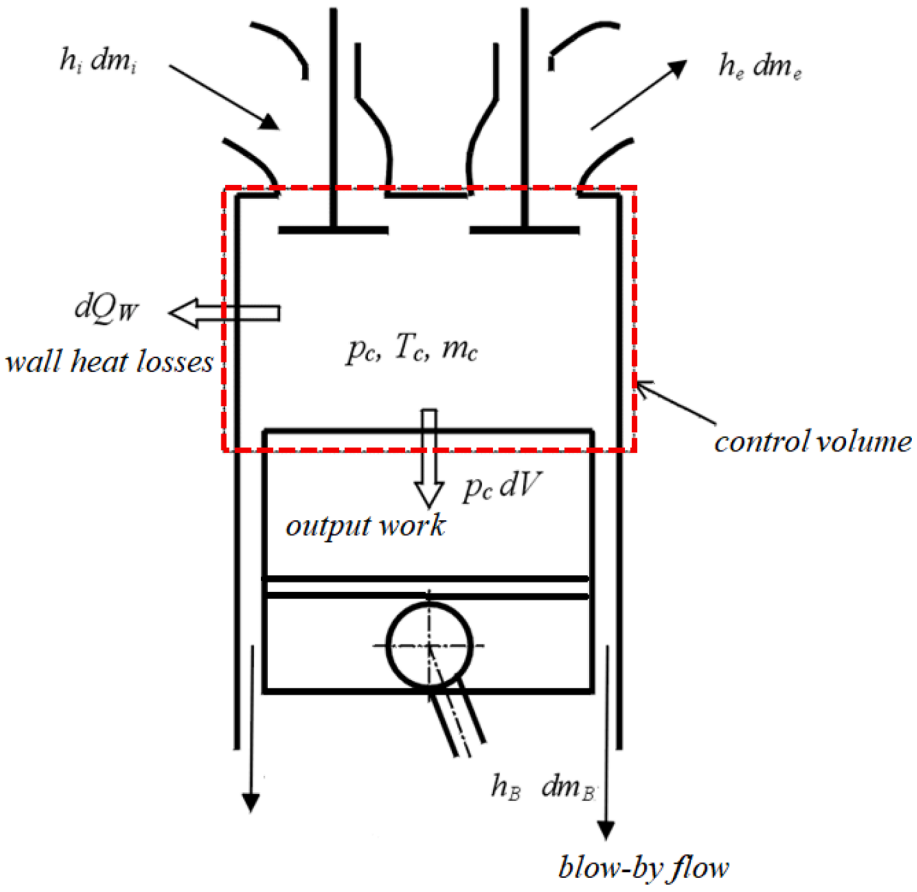

Fig. 4. A schematic sketch of cylinder.

with assigned fraction is calculated and stored in a library file to be used later in the combustion computations. The key parameters of elements with respective data values are presented in Table 4.

The AVL Boost interface is employed for modeling the different components and the fundamental process of combustion, mass/species transport, momentum, energy/heat transfer. The system configuration is an assembly of variety of components such as air-cleaner, cooling heat exchanger, cylinder, catalyst, and plenums.

In the multi-zone combustion models (internal and external mixture preparation) the NOx production models are activated and the NOx production model is tuned according to the NOx kinetic multiplier. The NOx model has two parameters. The NOx post-processing multiplier linearly increases calculated emissions. The NOx kinetic multiplier controls the sensitivity of the model; higher values lead to a more sensitive behavior [28,29].

3.1. Governing equations

According to the first law of thermodynamics, and considering the moving control volume within the piston-cylinder arrangement, the state of the system based on crank-angle is estimated as [30]:

$$\frac{d(m_c.u)}{d\theta} = -p_c.\frac{dV}{d\theta} + \frac{dQ_F}{d\theta} - \sum\frac{dQ_w}{d\theta} - h_B.\frac{dm_B}{d\theta} + \sum\frac{dm_i}{d\theta}.h_i - \sum\frac{dm_e}{d\theta}.h - q_{evp}.y.\frac{dm_{evp}}{dt} \quad (1)$$

The mass flow change with crank-angle is given as:

$$\frac{dm_c}{d\theta} = \sum\frac{dm_i}{d\theta} - \sum\frac{dm_e}{d\theta} - \frac{dm_B}{d\theta} + \frac{dm_{evp}}{dt} \quad (2)$$

where θ is crank-angle, p_c, m_c, V, u, y and q_{evp} are respectively cylinder pressure, cylinder mass, volume, specific internal energy, fuel evaporation fraction, and evaporation heat. Referring to Eq. (1), the variation in internal energy is the sum of piston work, fuel heat, wall heat losses, outflow of enthalpy, respectively. The in-cylinder gas composition is determined from the immediate combustion of the added fuel perfectly homogenized with the residual cylinder charge. Therefore, the air/fuel ratio decreases consistently from start of combustion onwards until the end of combustion. The following equation, together with Eq. (1), are employed to update pressure, temperature, and density using a Runge-Kutta method.

$$p_c = \frac{1}{V}.m_c.R_o.T_c \quad (3)$$

R_o is the universal gas constant. Upon finding the cylinder temperature, the above equation can be solved for obtaining the cylinder pressure. Fig. 4 presents a schematic of the cylinder for basic calcula-

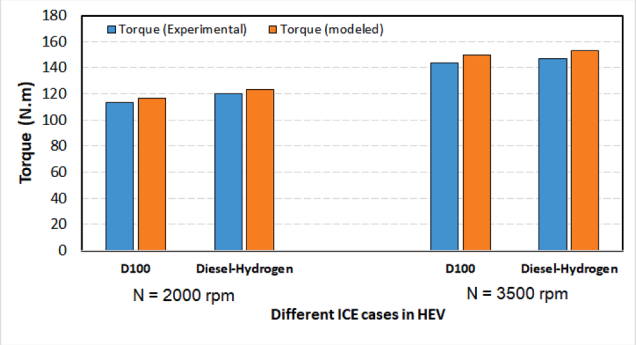

Fig. 5. Comparison of the model and measured data engine torque at different engine speeds and fueling cases.

tions of in-cylinder energy balance.

3.2. Classic species transport

Using the Classic Species Transport option conservation equations for combustion products (together with the air fuel ratio characteristic for them) and fuel vapor are solved.

The mass fraction of air is calculated from

$$y_{air} = 1 - y_{FV} - y_{CP} \tag{8}$$

where y_{air}, y_{FV}, and y_{CP} represent the mass fraction of air, fuel vapor, and combustion products, respectively. The air fuel ratio characteristic for the combustion products is calculated from

$$AFR_{CP} = \frac{y_{CP} - y_{FB}}{y_{FB}} \tag{9}$$

Where AFR_{CP} is the air/fuel ratio of the combustion products and y_{FB} gives the burned fuel mass fraction. For the calculation of the gas properties of exhaust gases the air fuel ratio is used as a measure for the gas composition. Air fuel ratio in this context means the air fuel ratio at which the combustion took place from which the exhaust gases under consideration originate. The composition of the combustion gases is obtained from the chemical equilibrium considering dissociation at the high temperatures in the cylinder.

4. Results and discussion

The results are presented for the hybrid ICE-Battery vehicle with the change in fuel type (diesel, hydrogen, and methanol) and the injection mode of the engine (RCCI and DCI). On the other hand, the battery condition (initial charge and cell number) are also considered in the presented results of this investigation.

The engine torque in HEV configuration is analyzed experimentally in [31] and then the simulated results are performed. The reliability of the design powertrain in this study for diesel and diesel-hydrogen operated ICE are compared in Fig. 5 with the measured results in two engine speeds of N = 2000 rpm and N = 3500 rpm for torque values. There is a slight deviation between the modeled and experimental result of the engine (below 3% gap) for the direct injection engine case for two fuel use in the system. The model performance thereby is ensured for the other cases considered in this research.

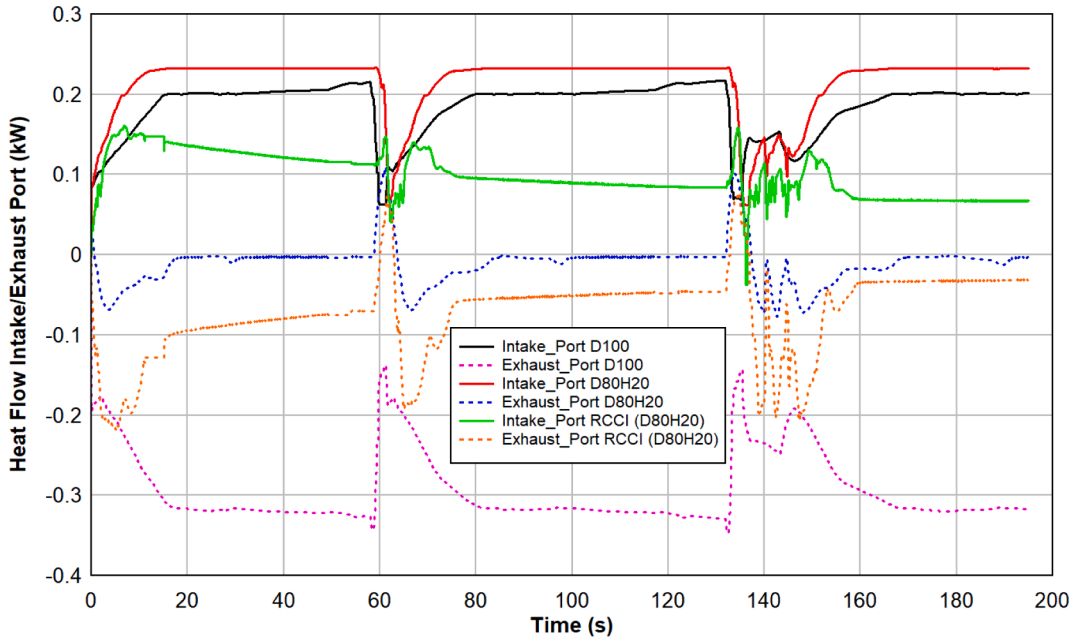

Fig. 6. Intake/Exhaust port heat flow over time for D100 and D80H20 (DCI and RCCI injection modes).

Table 5
Wall heat flow from the ICE for different fueling cases.

	Avg. Heat flow piston (kW), range (min,max)	Avg. Heat flow head (kW), range (min,max)	Avg. Heat flow liner (kW), range (min,max)
D100	−1.257, (−1.592,-0.325)	−0.839, (−1.063,-0.217)	−0.456, (−0.602,-0.084)
D80H20	−2.294, (−2.6,-0.427)	−1.531, (−1.741,-0.285)	−1.343, (−1.534,-0.194)
RCCI (D80H20)	−3.184, (−3.714,-0.55)	−2.125, (−2.479,-0.362)	−1.91, (−2.199,-0.266)

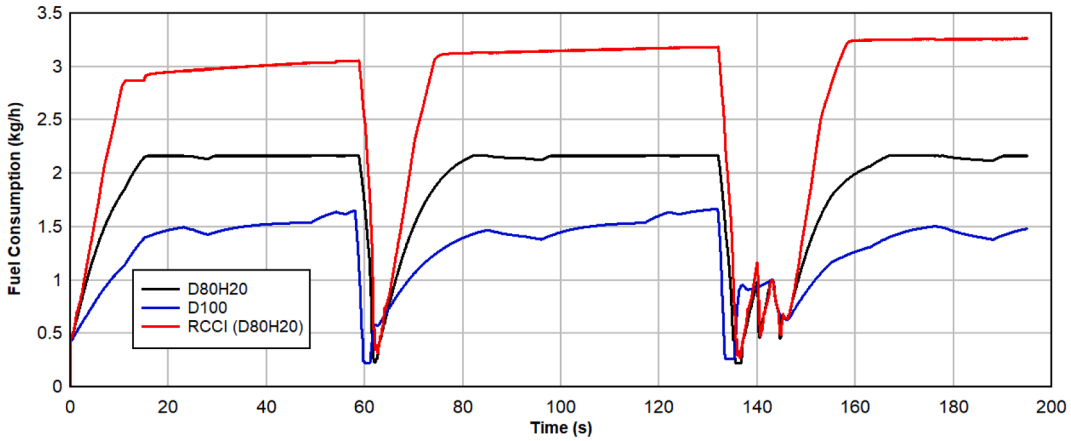

Fig. 7. Fuel consumption variation with time for D100 and D80H20 (DCI and RCCI injection modes) for NEDC drive cycle.

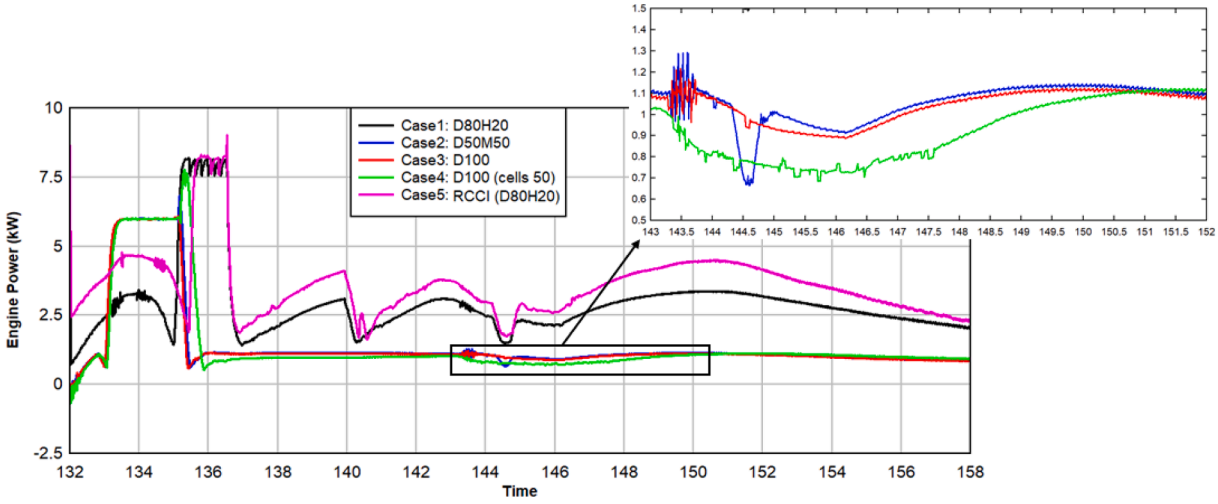

Fig. 8. Engine power with time for different fuel/injection tests and the battery capacity in accordance with NEDC driving format.

4.1. Thermal, performance, and emission evaluation of the ICE

The waste heat at the exhaust port of the hybrid powertrain for three different cases of D100, DCI of D80H20, and RCCI D80H20 are demonstrated in Fig. 6. It can be observed that using pure diesel in the engine has the highest heat flux from the exhaust valve, while applying the RCCI low temperature combustion with D80H20 composition of fuel has the lowest waste heat flow at the exhaust. Using 20% hydrogen causes dilution of the mixture and the lean gas + diesel mixture by a premixed blend can make a dramatic reduction in fuel chemical energy loss. The peak of the exhaust port heat flow is 0.347 kW for D100 conventional CI engine, while in the RCCI mode displays the peak of heat flow at the exhaust as much as 0.0776 kW. It can be seen that the overall heat flow for D100 shows outflux of heat while for DCI D80H20 it fluctuates around zero flux, and in the case of the RCCI the heat flow from the exhaust port has the overall negative amount. The integration of the battery with RCCI hybrid mode results in a significant thermal management and the fuel energy can be used without a considerable heat loss from the exhaust port. Moreover, the valley of the curve for D100 within 58–64 s and 133–137 s corresponds with the peak of the curves for the dual-fuel operation modes. The heat flow from the intake port is relatively higher than the heat flow that occurs in the exhaust port. Moreover, it is seen that the heat flow for the intake port of the RCCI is consistently reducing with time while for other cases the overall heat flow has a constant trend with time lapse. The addition of hydrogen to diesel causes lower heat flux from the engine and the RCCI dual injection mode leads to fuel energy saving due to low-temperature combustion and higher power efficiency.

The heat flow from different wall segments of the cylinder-piston along the variation range for the use of different fuels and injection cases in the ICE in the hybrid powering are tabulated in Table 5. Unlike the exhaust port heat transfer, the heat transfers and combustion losses from the walls for the D80H20 even the RCCI mode is higher than conventional diesel combustion. For the RCCI case, as reported by other literature [32], the peak temperature and combustion losses are higher than conventional diesel engine. Additionally, the engine speed by D80H20 and the consequent fuel consumption amount is comparatively more than diesel operated powertrain that results in higher energy generation in the cylinder. Accordingly, the higher heat transfer occurring by the RCCI D80H20 can be justified. Hydrogen has higher heating value and using this fuel in the combined fuel releases more energy and higher heat transfer in the form of the wall heat flux. According to Table 5, the heat flow from the piston has the highest share of the wall heat flux and the liner area heat loss is the lowest because the piston has the most surface area and the liner has the lowest surface area.

The fuel consumption in the engine over time for the NEDC drive cycle pattern for different fuel and combustion modes in the hybrid powertrain are exhibited in Fig. 7. As seen, the amount of fuel consumption for the conventional D100 is lower and when the RCCI D80H20 is applied the fuel consumption amount increases. In the RCCI mode of the ICE operation, there is more fuel consumption demand on

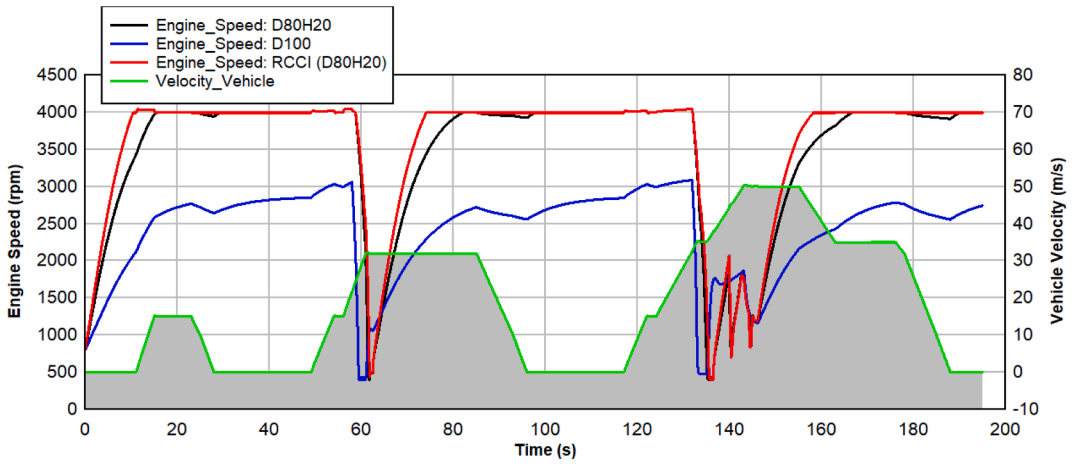

Fig. 9. Vehicle velocity profile and the corresponding engine speed for D100, D80H20, and the RCCI D80H20 operated ICE during NEDC driving time.

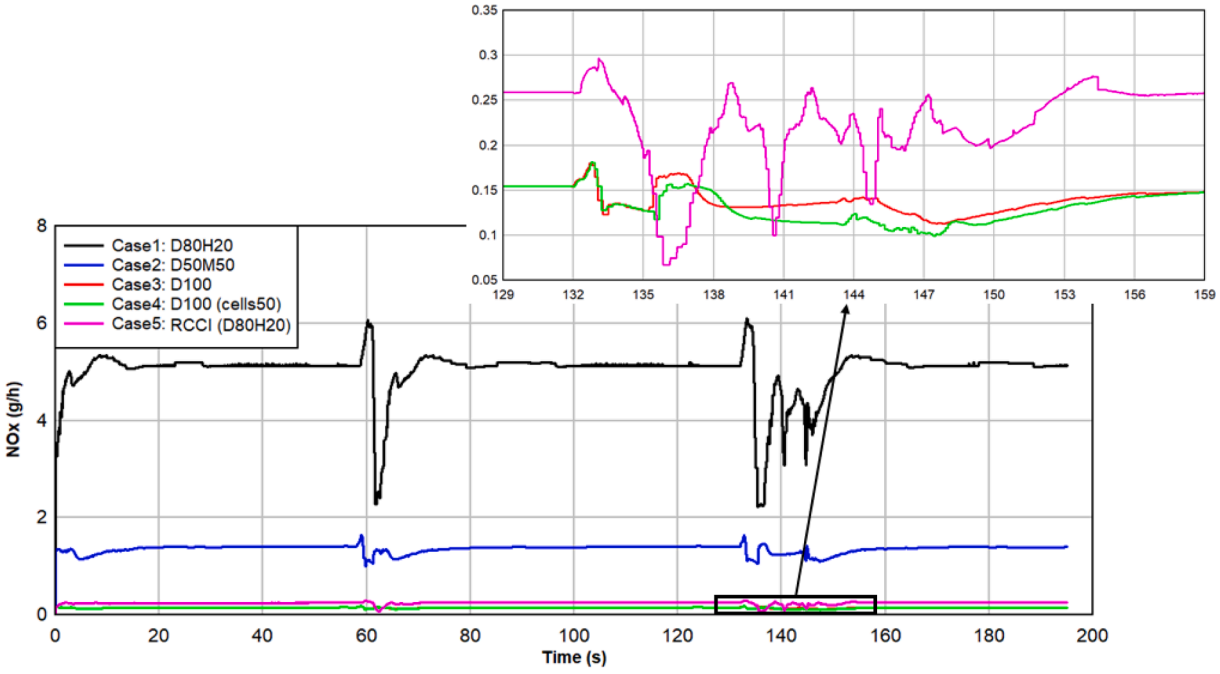

Fig. 10. NOx emission with time for different fuel/injection tests and the battery capacity in accordance with NEDC driving format.

the engine. The fuel consumption in the intervals of the acceleration (increasing the vehicle velocity) in the driving cycle around 60 s and 140 s for all fueling cases are close to each other. However, in the rest of the driving time the fuel consumption of the RCCI dual fuel consumption is twice the fuel consumption of diesel engine operation. This goes back to higher engine speed of both D80H20 operated engine compared to diesel fueled engine.

The engine power in power delivery time (out power not battery charging) for different cases are demonstrated in Fig. 8. The higher power delivery by the RCCI operation of the engine compared to D80H20 DCI can be observed. In addition, there can be seen that the RCCI has remarkably more power output compared to D100 conventional engine function in the hybrid vehicle with the battery. The controller makes the RCCI engine to operate at higher engine speed and deliver more power compared to D100 and on the other hand, as will be discussed later, lower battery or electrical consumption is required when the RCCI engine is used in the powertrain. The case of D50M50 is also provided for the comparison and it also produces lower engine power compared to D80H20 cases. The trend of the engine power for D50M50 is similar to D100 and does not affect the performance of the engine. Changing the charging and capacity of the battery can also slightly influence the engine power. The 50-cell battery size with 85% initial charging cause a negligible lower engine power from 136 to 150 s driving time, while in the subsequent time the engine power of low battery capacity is slightly more than 100-cell and full battery charging under D100 engine operation. The RCCI power output compared to DCI in D80H20 shows 16.32% better performance, which mainly comes from the premixed port fuel injection of low-reactive fuel i.e. hydrogen with air.

The engine speed and engine velocity profiles in three fueling scenarios are demonstrated in Fig. 9. The simultaneous variation of the engine speed and the vehicle velocity over time for the NEDC drive cycle are presented and it is shown that using D80H20 under the velocity profile and controller for the use of battery/ICE makes higher engine speed (4000 rpm) compared to D100 (~3000 rpm). The valley of the engine speed and the peaks of the vehicle velocity occurs in the same time spans around 60 s and 140 s to test different operational and dynamic modes of the vehicle. The RCCI D80H20 engine speed compared

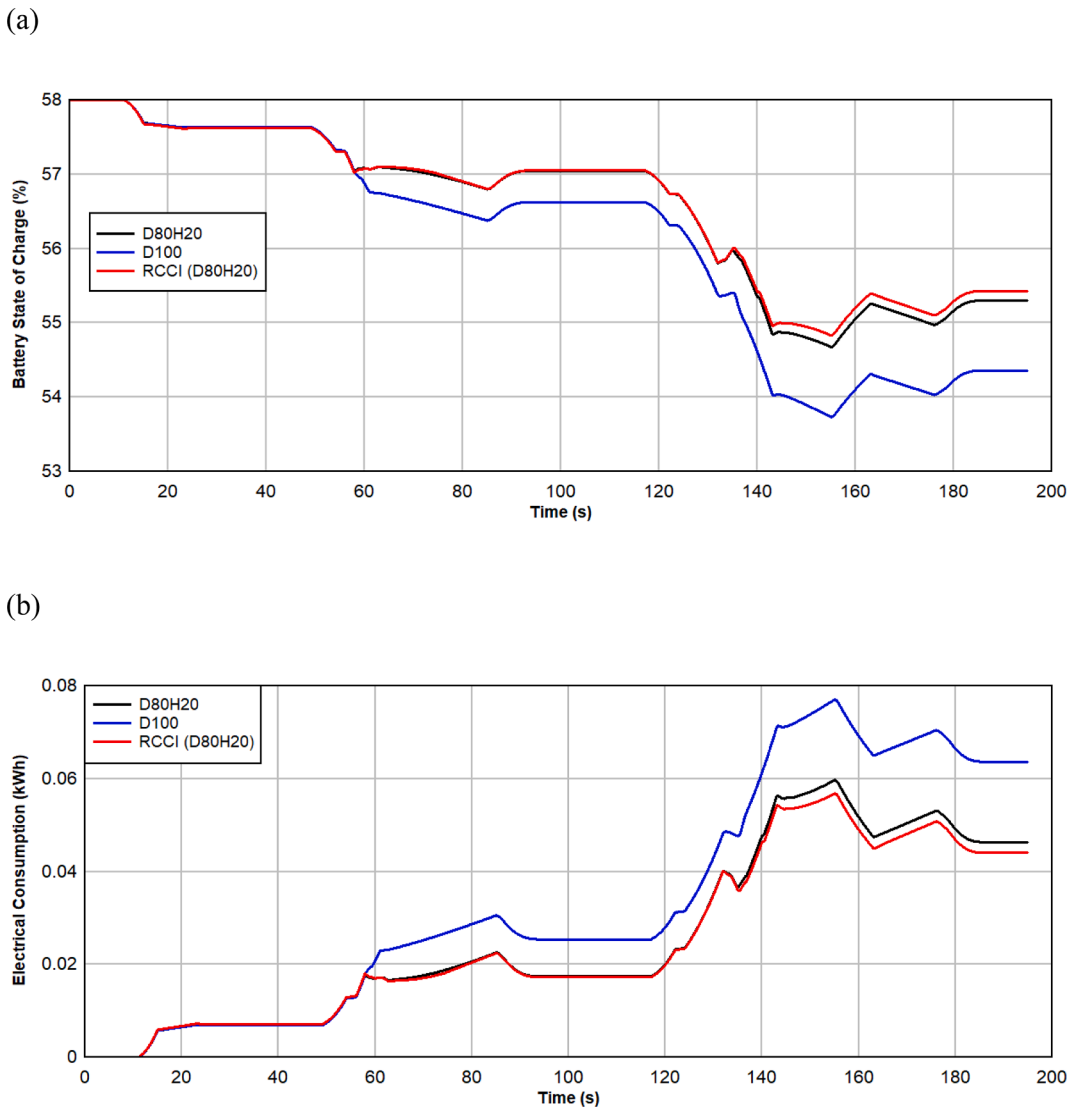

Fig. 11. (a) Battery SOC and (b) electrical consumption change over the driving time for D100, D80H20, and the RCCI D80H20 operated ICE.

to DCI D8H20 at initial engine speed up during three phases of 0, 60, and 150 s is a bit higher, while during the stable time, they are the same. The engine speed profile can explain the higher fuel consumption of the RCCI and the heat transfer related to the basic D100 engine operation mode. The engine model in the co-simulation platform is controlled by the fuel injection rate implemented with the ECU element. The ECU collects the load signals from the injectors, cylinders, engine, and turbocharger and sends the information to AVL engine-boost. These data cause the regulation of engine speed according to vehicle velocity profile as depicted in the following graph. This requires higher engne speed for dual-fuel operated engines.

The NOx emission variation during the drive cycle time for different cases of fueling (fuel type and injection configuration) and battery status are plotted and represented in Fig. 10. The interesting trend of NOx amount from the hybrid vehicle can be noticed such that the RCCI D80H20 has shown a striking lower amount than DCI D80H20 case. In D80H20 the injection is like D100 and the total fuel consisting of 80% diesel and 20% hydrogen are directly injected into the combustion chamber. While in the RCCI case, 20% hydrogen as low reactive fuel is injected into the duct and premixed with air and the rest of 80% diesel is injected directly into the combustion chamber and there are stratified mixture layers formed into the chamber. The low temperature combustion mode of dual-fuel injection in the RCCI design can drastically curb the NOx formation pathway especially in the hybrid power vehicle with battery/ICE. The D100 operated engine in conventional direct injection mode has lower NOx than DCI D80H20 since the hydrogen with higher LHV releases more heat. Thus under the same operational condition of the chamber, the temperature increases at DCI D80H20. The engine type of direct co-injection of D50M50 ranks the second highest NOx amount since methanol has the oxygen in its compound which forms the rich NO formation region and higher content of NOx. When the D100 engine coupled with battery of lower capacity the NOx is slightly lower than when the D100 engine is coupled with the full battery and 100 cells. This is because the engine power flows more toward the battery charging. In spite of the lowest NOx amount at 136 s for RCCI (~0.069 g/h), the D100 has overall lower NOx in the hybrid mode that can be attributed to interaction of battery-engine with the energy management strategy by the controller.

4.2. Battery performance

In this section the battery and electric connection characteristics of the HEV will be evaluated for main three cases of D100, D80H20, and the RCCI D80H20. The battery performance and the electric performance of the HEV under the evaluated parameters over time are represented in Fig. 11. The state of charge (SOC) of the battery in

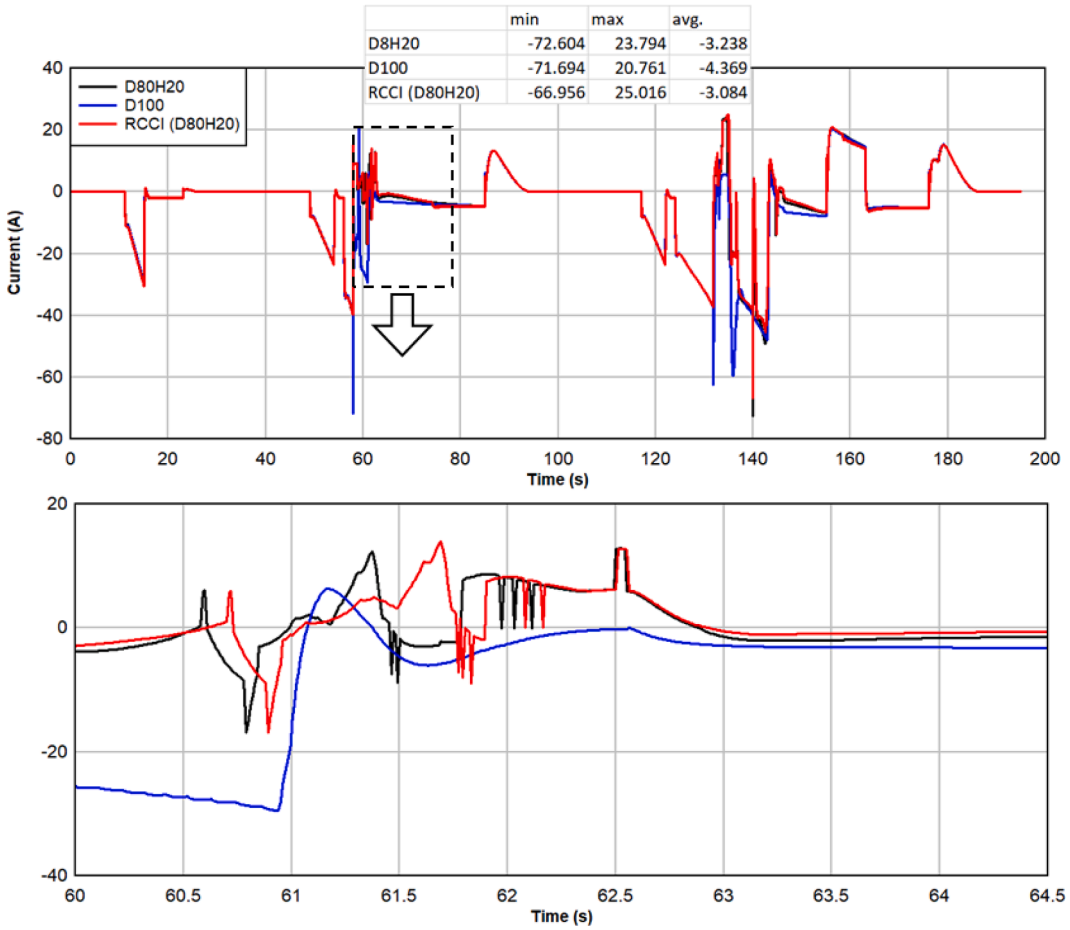

Fig. 12. Current variation for D100, D80H20, and the RCCI D80H20 operated ICE during NEDC driving time.

connection with different engine condition is lower once the engine is operated under D100 and the electrical consumption is the highest since the engine output efficiency in this case is lower and to maintain the desired power level more power of the battery must be consumed. The RCCI engine application priority is that it keeps the battery in the optimal charging condition over time and exhibits considerably lower NOx content compared to D80H20 case. The charging of battery in the RCCI over short time of 200 s reaches to 55.4% whereas for D100 the battery charging reduces to 54.3%. The improvement of HEV by the RCCI/battery compared to conventional design might not be considerable in terms of powering and the energy efficiency, but the mechanism of hybridizing power components can be further investigated. In the case of the RCCI incorporation to the battery in the parallel power arrangement, lower electric consumption of the battery is required and 26.23% saving in the peak electric consumption at 155 s occurs.

In the driveline including the mechanical systems and electric network, when the RCCI engine is hybridized, the battery performance is promoted during last driving period. This is explained by the powertrain connection of the AVL Boost component and Battery via the generator where the controller demand most of the required duty from the engine and thus the battery charging mode is preserved during the drive condition. The RCCI energy-efficient mechanism can make up for 0.02 kWh electrical consumption reduction and 1% more SOC. Although this is a low amount in electrical upgrade, the further modification of the RCCI and engine advancement can be a promising topic in the HEV technology.

The variation trend of the current in the electric connection from battery side when the ICE mode is designed in three different fueling and injection conditions are displayed in Fig. 12. The min, max, and average current for three cases of the ICE operation are also shown in tabulated format. The negative current towards the battery for the RCCI is the lowest while the maximum positive current from the battery in the case of the RCCI is the highest and reaches 25.016 A. The average current is negative and the highest negative current value is assigned to the time that the ICE operates with D100 (−4.36 A). The electric current of the battery and battery contribution in the driveline of the vehicle is more pronounced once the engine works in the RCCI mode. The negative current for charging the battery is more remarkable with the engine D100 especially at times of velocity increase as seen in the velocity profile. This conclusion that the stat of battery charge can be better maintained with the RCCI D80H20 engine is significant, although the system retrofit and tank/fueling line requires extra investigation. The negative current in the powering circuit for the case of D100 can be noted in the magnified view in the vehicle-accelerated zone of 60–64 s. The RCCI engine's fuel consumption in the mechanical line is in average 52.2% higher than diesel, but at the same time the electrical consumption decreases by 26.2% in this case since the RCCI coupled battery produces higher current.

In order to emphasize on the RCCI engine mode desirable effect on the battery performance, the battery power loss during the vehicle driving is shown for three different engine cases in Fig. 13. These power loss differences are more obvious during peak velocity around 60 s and 140 s where there is higher power loss when D100 is coupled with the battery. The RCCI D80H20 better fits with the battery co-powering in the HEV and assures the optimal battery operation and charging state compared to direct fuel injection engine in the hybrid vehicles. The battery SOC level during the drive cycle, lower power loss from the battery, and lower NOx are the direct result of using the RCCI engine coupled with the battery. The peak power loss during the first phase of acceleration is for D100 with 5.5096 kW and during the second

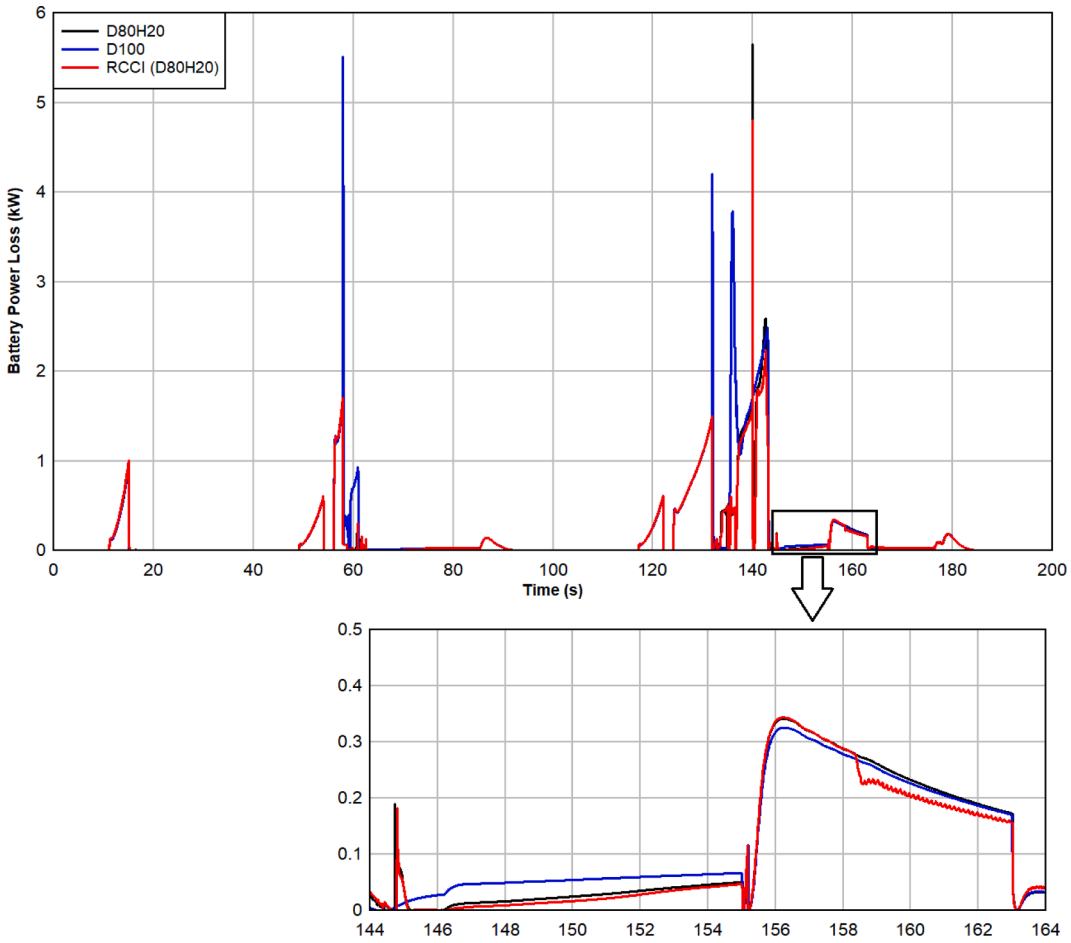

Fig. 13. Battery power loss variation for D100, D80H20, and the RCCI D80H20 operated ICE during NEDC driving time.

acceleration period attributes to DCI D80H20 with 5.64 kW.

Based on the obtained results, the HEV powertrain test cells can be equipped with the RCCI engine coupled with the battery or fuel cell for simultaneous ultra-emission reduction of NOx and extra power efficiency. The specific application of this study is the implementation of a hydrogen-diesel fueled engine in a hybrid electric vehicle in order to promote the engine efficiency and to eliminate its exhaust emissions. The application of the RCCI in hybrid mode can elongates the charging state of the battery, although implementation of dual fuel tank, injection line of direct/port injection, and engine modification in a real world powering system is unwieldy and requires the engineering effort for future vehicles. However, the limitation of dual-fueled engine in hybrid operation must be considered since the higher heat transfer expose the risk of overheating and a proper cooling system should be integrated.

5. Conclusion

The coupling of advanced combustion ICE with battery in HEV gives the following summarized points:

i. The battery power losses once switched to RCCI is lower and in D100 engine operation the peak battery losses are higher. This is in accordance with the better SOC condition when the battery is hybridized with D80H20 RCCI case, since the higher RCCI power output can charge and support the battery and prevent the battery power loss.
ii. The heat flow from the exhaust port for D80H20 is lower than D100, while the wall heat flux for D100 is larger than both D80H20 cases of DCI and RCCI. The effect of 20% hydrogen instead of diesel and injection method attribute in the heat losses from the combustion chamber in the HEV.
iii. From the engine power perspective, the RCCI case demonstrate the highest out power with 16.32% higher power generation compared to DCI of D80H20. This is because of air-hydrogen premixed port injection that increases the homogeneity of the mixture and better combustion quality compared to simultaneous co-injection.
iv. The RCCI engine in parallel HEV system produces ultra-low NOx amount with 0.2 g/h even when the engine runs at high-speed compared to DCI case. The reason is the low-temperature combustion of RCCI and hydrogen premixed combustion.
v. In the hybrid mode of ICE/battery, when the powertrain operates with RCCI, the max current is achieved with 25.016 A while the min current of 20.761 A is established with engine that runs with D100.
vi. It is recommended that the battery is linked with dual-fuel port + direct injection (RCCI) rather than direct compression ignition or convention diesel combustion (CDC).
vii. From the R&D point of view, the engine behavior in a hybrid and non-hybrid driveline is different. Such that D100 in hybrid mode can operate better than RCCI in terms of thermal efficiency and NOx control.

CRediT authorship contribution statement

Hadi Taghavifar: Conceptualization, Data curation, Formal analysis, Investigation, Methodology, Project administration, Software, Supervision, Writing – original draft.

Declaration of Competing Interest

The authors declare that they have no known competing financial interests or personal relationships that could have appeared to influence the work reported in this paper.

Data availability

The data that has been used is confidential.

References

[1] Chen D, Jiang J, Kim GH, Yang C, Pesaran A. Comparison of different cooling methods for lithium ion battery cells. Appl Therm Eng 2016;94:846–54.
[2] Qiao Q, Zhao F, Liu Z, He X, Hao H. Life cycle greenhouse gas emissions of Electric Vehicles in China: Combining the vehicle cycle and fuel cycle. Energy 2019;177:222–33.
[3] Duan H, Jia M, Chang Y, Liu H. Experimental study on the influence of low-temperature combustion (LTC) mode and fuel properties on cyclic variations in a compression-ignition engine. Fuel 2019;256:115907.
[4] Kokjohn SL, Hanson RM, Splitter DA, Reitz RD. Fuel reactivity controlled compression ignition (RCCI): a pathway to controlled high-efficiency clean combustion. Int J Engine Res 2011;12(3):209–26.
[5] Benajes J, García A, Monsalve-Serrano J, Sari RL. Fuel consumption and engine-out emissions estimations of a light-duty engine running in dual-mode RCCI/CDC with different fuels and driving cycles. Energy 2018;157:19–30.
[6] Taghavifar H, Anvari S, Parvishi A. Benchmarking of water injection in a hydrogen-fueled diesel engine to reduce emissions. Int J Hydrogen Energy 2017;42(16):11962–75.
[7] Taghavifar H, Nemati A, Salvador FJ, De la Morena J. 1D energy, exergy, and performance assessment of turbocharged diesel/hydrogen RCCI engine at different levels of diesel, hydrogen, compressor pressure ratio, and combustion duration. Int J Hydrogen Energy 2021;46(42):22180–94.
[8] Pan L, Hu E, Deng F, Zhang Z, Huang Z. Effect of pressure and equivalence ratio on the ignition characteristics of dimethyl ether-hydrogen mixtures. Int J Hydrogen Energy 2014;39(33):19212–23.
[9] Zhu Z, Mu Z, Wei Y, Du R, Liu S. Experimental evaluation of performance of heavy-duty SI pure methanol engine with EGR. Fuel 2022;325:124948.
[10] Duraisamy G, Rangasamy M, Govindan N. A comparative study on methanol/diesel and methanol/PODE dual fuel RCCI combustion in an automotive diesel engine. Renew Energy 2020;145:542–56.
[11] Luján JM, García A, Monsalve-Serrano J, Martínez-Boggio S. Effectiveness of hybrid powertrains to reduce the fuel consumption and NOx emissions of a Euro 6d-temp diesel engine under real-life driving conditions. Energ Conver Manage 2019;199:111987.
[12] García A, Monsalve-Serrano J, Sari R, Dimitrakopoulos N, Tunér M, Tunestål P. Performance and emissions of a series hybrid vehicle powered by a gasoline partially premixed combustion engine. Appl Therm Eng 2019;150:564–75.
[13] Taghavifar H. Fuel cell hybrid range-extender vehicle sizing: Parametric power optimization. Energy 2021;229:120786.
[14] García A, Monsalve-Serrano J, Martinez-Boggio S, Gaillard P, Poussin O, Amer AA. Dual fuel combustion and hybrid electric powertrains as potential solution to achieve 2025 emissions targets in medium duty trucks sector. Energ Conver Manage 2020;224:113320.
[15] Yang L, Wang W, Yang C, Du X, Zhang W. Online mixed-integer optimal energy management strategy for connected hybrid electric vehicles. J Clean Prod 2022;374:133908.
[16] Wu C, Ruan J, Cui H, Zhang B, Li T, Zhang K. The application of machine learning based energy management strategy in multi-mode plug-in hybrid electric vehicle, part I: Twin Delayed Deep Deterministic Policy Gradient algorithm design for hybrid mode. Energy 2023;262:125084.
[17] Wang F, Xia J, Cai Y, Guo J. Novel energy management strategy for a dual-motor hybrid electric vehicle considering frequency of mode transitions. Energ Conver Manage 2022;269:116106.
[18] García A, Monsalve-Serrano J, Lago Sari R, Martinez-Boggio S. Energy sustainability in the transport sector using synthetic fuels in series hybrid trucks with RCCI dual-fuel engine. Fuel 2022;308:122024.
[19] Climent H, Dolz V, Pla B, González-Domínguez D. Analysis on the potential of EGR strategy to reduce fuel consumption in hybrid powertrains based on advanced gasoline engines under simulated driving cycle conditions. Energ Conver Manage 2022;266:115830.
[20] Benajes J, García A, Monsalve-Serrano J, Martínez-Boggio S. Emissions reduction from passenger cars with RCCI plug-in hybrid electric vehicle technology. Appl Therm Eng 2020;164:114430.
[21] AVL CRUISE., 2011. Users guide, AVL list GmbH, Graz, Austria, Document no. 04.0104.2011, Edition 06.2011.
[22] Wang S, Huang X, López JM, Xu X, Dong P. Fuzzy adaptive-equivalent consumption minimization strategy for a parallel hybrid electric vehicle. IEEE Access 2019;7:133290–303.
[23] Varga BO, Iclodean C, Mariasiu F. Electric and hybrid buses for urban transport: energy efficiency strategies. Springer; 2016.
[24] Varga BO, Mariasiu F, Moldovanu D, Iclodean C. Electric and plug-in hybrid vehicles. Cham: Springer International Publishing; 2015.
[25] Stone R, Ball J. Automotive engineering fundamentals. SAE; 2004i–xv.
[26] Taghavifar H. Experimental and numerical engine cycle setup for a dual fuel hydrogen, methane, and hythane with diesel to assess the effect of water injection and nozzle geometry. Environ Prog Sustain Energy 2022:e13936.
[27] Petranović Z, Sjerić M, Taritaš I, Vujanović M, Kozarac D. Study of advanced engine operating strategies on a turbocharged diesel engine by using coupled numerical approaches. Energ Conver Manage 2018;171:1–11.
[28] Taghavifar H, Mazari F. 1D diesel engine cycle modeling integrated with MOPSO optimization for improved NOx control and pressure boost. Energy 2022;247:123517.
[29] Pattas K, Häfner G. Formation of nitrogen oxides in gasoline engine combustion. Engine Technol Z 1973;34(12).
[30] A. Boost, Theory manual (avl boost v.2018.1), AVL List Gmbh, Graz-Austria.
[31] Arat HT. Alternative fuelled hybrid electric vehicle (AF-HEV) with hydrogen enriched internal combustion engine. Int J Hydrogen Energy 2019;44(34):19005–16.
[32] Olmeda P, Garcia A, Monsalve-Serrano J, Sari RL. Experimental investigation on RCCI heat transfer in a light-duty diesel engine with different fuels: Comparison versus conventional diesel combustion. Appl Therm Eng 2018;144:424–36.